Manuscript prepared for Atmos. Chem. Phys.
with version 2014/09/16 7.15 Copernicus papers of the LaTeX class copernicus.cls.
Date: 13 July 2015

On the use of satellite-derived CH_4:CO_2 columns in a joint inversion of CH_4 and CO_2 fluxes

S. Pandey[1,2], S. Houweling[1,2], M. Krol[1,2,3], I. Aben[2], and T. Röckmann[1]

[1]Institute for Marine and Atmospheric Research Utrecht, Utrecht University, the Netherlands
[2]SRON Netherlands Institute for Space Research, Utrecht, the Netherlands
[3]Wageningen University, Wageningen, the Netherlands

Correspondence to: S. Pandey (s.pandey@uu.nl)

Abstract. We present a method for assimilating total column CH_4:CO_2 ratio measurements from satellites for inverse modeling of CH_4 and CO_2 fluxes using the variational approach. Unlike conventional approaches, in which retrieved CH_4:CO_2 are multiplied by model derived total column CO_2 and only the resulting CH_4 is assimilated, our method assimilates the ratio of CH_4 and CO_2 directly and is therefore called the ratio method. It is a dual tracer inversion, in which surface fluxes of CH_4 and CO_2 are optimized simultaneously. The optimization of CO_2 fluxes turns the hard constraint of prescribing model derived CO_2 fields into a weak constraint on CO_2, which allows us to account for uncertainties in CO_2. The method has been successfully tested in a synthetic inversion setup. We show that the ratio method is able to reproduce assumed true CH_4 and CO_2 fluxes starting from a prior, which is derived by perturbing the true fluxes randomly. We compare the performance of the ratio method with that of the traditional proxy approach and the use of only surface measurements for estimating CH_4 fluxes. Our results confirm that the optimized CH_4 fluxes are sensitive to the treatment of CO_2, and that hard constraints on CO_2 may significantly compromise results that are obtained for CH_4. We find that the relative performance of ratio and proxy methods have a regional dependence. The ratio method performs better than the proxy method in regions where the CO_2 fluxes are most uncertain. However, both ratio and proxy methods perform better than the surface measurement-only inversion, confirming the potential of space borne measurements for accurately determining fluxes of CH_4 and other GHGs.

1 Introduction

In the past century, the concentrations of many potent greenhouse gases (GHGs) have increased in the atmosphere due to anthropogenic activities. The atmospheric dry air mole fraction of the greenhouse gas methane ($\mathrm{CH_4}$), which has a global warming potential of 28–34 on a $100\,\mathrm{year}$ time horizon (Myhre et al., 2013), has increased from $700\,\mathrm{ppb}$ during the pre-industrial era to $\approx 1800\,\mathrm{ppb}$ today (Ferretti et al., 2005). These atmospheric concentrations are unprecedented during at least the last $650\,000\,\mathrm{years}$ (Spahni et al., 2005). The direct radiative forcing caused by the increase of methane since pre-industrial times is $+0.48 \pm 0.05\,\mathrm{W\,m^{-2}}$ (Myhre et al., 2013), which amounts to $20\,\%$ of the present day cumulative radiative forcing due to all anthropogenic GHGs. Methane also influences atmospheric chemistry and it is an important control on the oxidising capacity of the atmosphere. Further details about the methane budget can be found in Kirschke et al. (2013). The atmospheric growth rate of methane has varied considerably in the last two decades (Bousquet et al., 2006; Nisbet et al., 2014). Causes of these variations are still not fully understood, which calls for better monitoring of its sources and sinks using both top-down and bottom-up studies.

The top-down approach uses inverse modeling techniques to reduce the uncertainty in the bottom-up derived emission estimates on the basis of atmospheric measurements of $\mathrm{CH_4}$. In the past, several studies applied the top-down method assimilating surface-based measurements from global monitoring networks operated by National Oceanic and Atmospheric Administration–Earth System Research Laboratory (NOAA/ESRL), the Advanced Global Atmospheric Gases Experiment, and Commonwealth Scientific and Industrial Research Organization (Bousquet et al., 2011, 2006; Hein et al., 1997; Houweling et al., 1999). However, due to poor spatial coverage of the surface measurement sites, such inversions are effective in constraining the fluxes at sub-continental scales at best (Houweling et al., 1999).

Total column measurements of $\mathrm{CO_2}$ and $\mathrm{CH_4}$ (X_{CH4} and X_{CO2}) from satellites have proven valuable for inversion studies of $\mathrm{CH_4}$ and $\mathrm{CO_2}$, especially in regions where surface measurement sites are sparse (Basu et al., 2014, 2013; Bergamaschi and Frankenberg, 2009; Houweling et al., 2014). For example, atmospheric retrievals from the Thermal and Near infrared Sensor for carbon Observations (TANSO) onboard the GOSAT (Greenhouse gases Observering SATellite, Kuze et al. (2009)) have provided valuable constraints on the fluxes of $\mathrm{CH_4}$ and $\mathrm{CO_2}$ (Basu et al., 2013; Fraser et al., 2013). The $\mathrm{CH_4}$ absorption band at 1.6 micron allows retrieval of its atmospheric concentration with high sensitivity to the planetary boundary layer, where the signals of the sources are strongest. Besides a good sensitivity to the sources, the quality of the inversion-derived $\mathrm{CH_4}$ budget depends strongly on the precision and accuracy of the measurements. It has been shown that systematic errors on regional or seasonal scales of less than $1\,\%$ can jeopardize the usefulness of satellite measured $\mathrm{CH_4}$ columns for estimating $\mathrm{CH_4}$ budget (Bergamaschi et al., 2007).

High quality X_{CH4} and X_{CO2} retrievals require accurate knowledge of the light-path of the photons that are measured by the satellite. Scattering of light on atmospheric particles (aerosol particles and cloud droplets) may lead to significant light-path perturbations. The accuracy of X_{CH4} retrievals depends to a large extent on how well the retrieval technique can account for such scattering induced perturbations. A commonly used technique is the so-called proxy method, which was originally developed for retrieving X_{CH4} and X_{CO2} using nearby spectral windows from SCIAMACHY (Frankenberg et al., 2005). Since atmospheric scattering affects both compounds in a similar way, light-path errors largely cancel out in the ratio. The retrieval-derived ratio ($\frac{X^{\mathrm{obs}}_{\mathrm{CH4}}}{X^{\mathrm{obs}}_{\mathrm{CO2}}}$) is multiplied with a priori knowledge of atmospheric $\mathrm{CO_2}$ derived from a model ($X^{\mathrm{model}}_{\mathrm{CO2}}$) to generate proxy column measurements of $\mathrm{CH_4}$ ($X^{\mathrm{proxy}}_{\mathrm{CH4}}$) (Eq. 1).

$$X^{\mathrm{proxy}}_{\mathrm{CH4}} = \frac{X^{\mathrm{obs}}_{\mathrm{CH4}}}{X^{\mathrm{obs}}_{\mathrm{CO2}}} \times X^{\mathrm{model}}_{\mathrm{CO2}}, \tag{1}$$

$X^{\mathrm{model}}_{\mathrm{CO2}}$ is usually derived from the results of a $\mathrm{CO_2}$ inversion using the surface measurements, such as CarbonTracker (Peters et al., 2007). It is assumed that: (1) $\mathrm{CO_2}$ exhibits comparatively smaller unknown variations in the atmosphere than $\mathrm{CH_4}$, and (2) residual differences in scattering between the spectral windows of $\mathrm{CO_2}$ (1562 to 1585 nm) and $\mathrm{CH_4}$ (1630 to 1670 nm) used in the retrieval are insignificant. Hence, $\mathrm{CO_2}$ is used as proxy for changes in the light-path. Schepers et al. (2012) discuss the performance of GOSAT RemoTeC proxy retrieval in detail. This retrieval dataset has been used successfully in inversion studies for optimizing $\mathrm{CH_4}$ fluxes (Alexe et al., 2014; Monteil et al., 2013). In these studies the error in $X^{\mathrm{model}}_{\mathrm{CO2}}$ is assumed to be negligible compared to retrieval error in $\frac{X^{\mathrm{obs}}_{\mathrm{CH4}}}{X^{\mathrm{obs}}_{\mathrm{CO2}}}$. However, with the gradually improving quality of the GOSAT retrievals, errors in model-derived $\mathrm{CO_2}$ may become a bottleneck for improving inversion-derived $\mathrm{CH_4}$ fluxes (Schepers et al., 2012).

In some regions, the sparse network of surface measurement sites does not provide sufficient constraints on $\mathrm{CO_2}$ fluxes, leading to possible biases in $X^{\mathrm{model}}_{\mathrm{CO2}}$ (Schepers et al., 2012). In this study we investigate a new method, called the ratio method, which circumvents the use of $X^{\mathrm{model}}_{\mathrm{CO2}}$ by directly assimilating the retrieved ratio of total column $\mathrm{CH_4}$ and $\mathrm{CO_2}$ into an inversion that optimizes $\mathrm{CH_4}$ and $\mathrm{CO_2}$ fluxes simultaneously. Thus, in the ratio method Eq. (1) is replace by

$$X_{\mathrm{ratio}} = \frac{X^{\mathrm{obs}}_{\mathrm{CH4}}}{X^{\mathrm{obs}}_{\mathrm{CO2}}} \tag{2}$$

Our motivation for implementing the ratio method is to find a representation of $\mathrm{CO_2}$ in the inversion system, that is more consistent with both X_{ratio} and $\mathrm{CO_2}$ surface measurements. Also, X_{ratio} is less biased and has a larger number of measurements than $\mathrm{XCH_4}$ and $\mathrm{XCO_2}$ full-physics retrievals (Fraser et al., 2014). Fraser et al. (2014) introduced the assimilation of satellite retrieved X_{ratio} in a maximum a posteriori (MAP) inversion system for constraining the surface fluxes of $\mathrm{CH_4}$ and $\mathrm{CO_2}$. However, the transport model and inversion method used in their study are different from the ones used here.

We perform Observing System Simulation Experiments (OSSEs) to test the performance of the ratio method for reproducing the assumed true fluxes of $\mathrm{CH_4}$ and $\mathrm{CO_2}$. The results are compared with inversions using proxy retrievals and only surface measurements. In the following Sect. 2, we elaborate on our inverse modeling setup, and describe our OSSE experiments. In Sect. 3, we analyze and compare the inversion-estimated posterior fluxes of CH_4 and CO_2. In Sect. 4, we further discuss the significance and limitations of our findings and evaluate the future potential of the ratio method for application in inversion studies, leading to our final conclusions.

2 Method

2.1 Inverse modeling

We use the TM5-4DVAR inversion system in this study. It comprises of the Tracer Transport Model version 5 (TM5, Krol et al., 2005) coupled to a variational data assimilation system (4DVAR, Meirink et al., 2008). TM5 simulates the spatio-temporal distribution of a tracer in the atmosphere for a given set of fluxes and initial concentrations that are prescribed as boundary conditions to the model. We have set up a dual tracer version of TM5-4DVAR for simultaneous simulation of CH_4 and CO_2. By combining the output of the two tracers, this model allows us to simulate X_{ratio} (see Eq. 2). The 4DVAR technique uses model calculated and observational dataset of X_{ratio} to optimize a state vector $\boldsymbol{x}$, consisting of surface fluxes of CH_4 and CO_2. The optimum is found by minimizing a Bayesian cost function, defined as

$$J(\boldsymbol{x}) = \frac{1}{2}(\boldsymbol{x}-\boldsymbol{x}_b)^T\mathbf{B}^{-1}(\boldsymbol{x}-\boldsymbol{x}_b) + \frac{1}{2}(\boldsymbol{y}-\boldsymbol{H}\boldsymbol{x})^T\mathbf{R}^{-1}(\boldsymbol{y}-\boldsymbol{H}\boldsymbol{x}) \quad (3)$$

where $\boldsymbol{x}_b$ is the a priori knowledge of $\boldsymbol{x}$, and $\boldsymbol{H}$ is the observation operator, which converts the output of the model, forced by $\boldsymbol{x}$, to corresponding mixing ratios at the measurement sites of $\boldsymbol{y}$. Hence, $\boldsymbol{H}\boldsymbol{x}$ represents the model simulated counterpart of the observation vector $\boldsymbol{y}$. $\mathbf{R}$ and $\mathbf{B}$ are error covariance matrices for $\boldsymbol{y}-\boldsymbol{H}\boldsymbol{x}$ and $\boldsymbol{x}_b$, respectively. Each iteration of TM5-4DVAR is composed of a forward and an adjoint TM5 run (Errico, 1997). The forward run is used to calculate the value of the cost function for a trial state vector $\boldsymbol{x}_j$ (using Eq. 3). The adjoint run provides the corresponding cost function gradient ($\nabla J(\boldsymbol{x})$). At the end of each inversion iteration j, $\nabla J(\boldsymbol{x}_j)$ and the state vector $\boldsymbol{x}_j$ are fed into an optimizer module to calculate the state vector for the next iteration ($\boldsymbol{x}_{j+1}$). For linear inverse problems we use the conjugate gradient optimizer (CONGRAD, Lanczos, 1950), that has been used extensively for linear inversion problems (Basu et al., 2013; Houweling et al., 2014; Monteil et al., 2011, 2013). Mathematically, it has the fastest convergence rate for linear inversions, but it may perform poorly for non-linear inversions

Our inversion setup for the proxy approach is linear. However, for the new ratio method the operator $\boldsymbol{H}$ includes Eq. (2), and hence, the inversion becomes non-linear making M1QN3 a more suitable optimizer than CONGRAD. M1QN3 is a quasi-Newton algorithm based optimizer (Gilbert and Lemaréchal, 1989), which is commonly used in non-linear inverse modeling (Cressot et al., 2014; Krol et al., 2013; Muller and Stavrakou, 2005). It has the ability to rebuild the second derivative of the cost functions several times during its descent to minimum, and therefore, performs better for non-linear inverse problems.

To compare the difference in convergence between M1QN3 and CONGRAD, we performed additional proxy inversions using both optimization methods (see Appendix A). We find that M1QN3 has a slower convergence rate in comparison to CONGRAD, and therefore the number of iterations needed to find the inversion solution is generally higher. Another drawback of the M1QN3 algorithm that is available to us is that, unlike CONGRAD, it provides no information about the posterior flux uncertainties in a straightforward way.

2.2 Truth and prior

The assumed true CH_4 and CO_2 fluxes for our inversion setup are taken from Houweling et al. (2014) and Basu et al. (2013), respectively. The generation of pseudo observations $\boldsymbol{y}$ is explained in the next section. Concerning the state vector $\boldsymbol{x}$, CH_4 fluxes are optimized for a single category representing the net flux from all the contributing processes at the surface, discretized per model grid box and per month. For CO_2, we optimize for fluxes from the biosphere and the ocean, discretized in time and space like methane. We do not optimize emissions from other categories like biomass burning and fossil fuel usage, as they are assumed to have relatively small uncertainties. Table 1 shows the parameters used to calculate the error covariance matrix $\mathbf{B}$ for the prior fluxes. We assume no prior correlation between flux categories of CO_2 biosphere, CO_2 oceanic and CH_4 total. The spatiotemporal covariance components for each category were included in $\mathbf{B}$. For details about this implementation of $\mathbf{B}$ in our inversion see Basu et al. (2013). We use one set of prior fluxes $\boldsymbol{x}_b$ for all inversions, which was created by adding Gaussian noise to the true CH_4 and CO_2 fluxes. The noise is generated using the a priori flux uncertainties accounting for spatial and temporal error correlations, as described in Chevallier et al. (2007). Figure 2 shows the time series of the true and prior fluxes for four Transcom regions (explained in Fig. 1). As can be seen, the assumptions regarding the a priori flux uncertainties lead to realistic deviations from the truth in terms of seasonality and net monthly flux.

2.3 Measurements

Pseudo surface observations are generated from a forward run of TM5 using the “true” fluxes as boundary conditions, and they are sampled at coordinates and times of samples collected by cooperative flask-sampling network run by NOAA/ESRL (Dlugokencky et al., 2009) in the period 1 June 2009 to 30 May 2010 at the sites shown in Fig. 1. In total, we use 3934 surface measurements of CH_4 (from 93 sites) and 1184 measurements of CO_2 (from 85 sites). Similarly, synthetic total column measurements are generated at the times and locations of the GOSAT RemoTeC v1.9 proxy satellite retrievals for the same time period (Schepers et al., 2012). We do not sample GOSAT data for cloud free conditions, and therefore assimilate a rather optimistic number of GOSAT measurements. However, satellites such as Sentinel-5 will provide a comparable amount of data. The forward run of TM5 calculates 25 layer vertical model profiles at the retrieval coordinates. These profiles are converted into the corresponding total columns using the retrieval derived averaging kernels (see e.g. Monteil et al., 2013). In total, we use 443 523 GOSAT total column retrievals of both $\mathrm{CH_4}$ and $\mathrm{CO_2}$ (see Fig. 3).

The observational part of the cost function is calculated by weighing the mismatch between the model simulations and measurements ($\boldsymbol{y}-\boldsymbol{H}\boldsymbol{x}$) with the data error covariance matrix $\mathbf{R}$. The diagonal terms of $\mathbf{R}$ are the squared sum of measurement uncertainty and model representation error. We assume no correlation between the measurements. Therefore, all the non-diagonal terms of $\mathbf{R}$ are set to zero. The model representation error is the error made by our finite resolution model in simulating a sample at a specific location. Its size scales with the subgrid concentration variability, and is calculated using the local concentration gradient simulated by the model. Further details about the calculation of the model representation error in our setup can be found in Basu et al. (2013). For the measurement uncertainties we follow the recommendations of the data providers. For the GOSAT retrieved total column ratios, the uncertainty was calculated by error propagation of the instrument's measurement noise of the $\mathrm{CH_4}$ and $\mathrm{CO_2}$ total columns given in retrieval data set. The uncertainties of proxy $\mathrm{CH_4}$ total columns are also calculated in similar ways. In principle, they should be the ratio uncertainties plus the $X^{\mathrm{model}}_{\mathrm{CO2}}$ uncertainty (see Eqs. 1 and 2). However, the uncertainties from $X^{\mathrm{model}}_{\mathrm{CO2}}$ are neglected in real world applications, and we follow the same procedure. Hence, in our experiment, the ratio and proxy columns have the same relative uncertainties. For computational efficiency, we assume no correlation between the measurements (i.e. all the non-diagonal term of $\mathbf{R}$ are set to zero).

Formally, we should perturb the pseudo measurements with noise according to the data covariance matrix $\mathbf{R}$, following the same procedure as for the a priori fluxes. However, to catch the mean behavior one would have to do several inversions with different noise realizations. This multi-inversion mean would correspond to the results of a single inversion without noise. For this reason we do not perturb the data. It should also be noted that satellite measurements are simulated using the same prior profiles as used for the real RemoTeC GOSAT retrievals. Since the same prior profile is used in the inversion and in the generation of pseudo data, its contribution cancels out in the model data mismatch and therefore does not influence the results.

In the ratio inversion, the GOSAT measurements are in terms of X_{ratio}, whereas the output of the transport model is in terms of $X^{\mathrm{obs}}_{\mathrm{CH4}}$ and $X^{\mathrm{obs}}_{\mathrm{CO2}}$. The observation operator $\boldsymbol{H}$ transforms the absolute columns to column ratios using Eq. (2). For calculating the gradient of $J(\boldsymbol{x})$, the adjoint of $\boldsymbol{H}$ is needed for propagating the sensitivities of the cost function from X_{ratio} to the corresponding sensitivities of $X^{\mathrm{obs}}_{\mathrm{CH4}}$ and $X^{\mathrm{obs}}_{\mathrm{CO2}}$. This adjoint is derived by applying the adjoint coding rules described in Errico (1997). It should be noted that the problem is only weakly non-linear since the values of

$X^{\text{obs}}_{\text{CO2}}$ vary in the narrow range of ≈ 350–$400\,\text{ppm}$ in our calculations, and the inversion-derived adjustments to $X^{\text{obs}}_{\text{CO2}}$ are only a small fraction of that range.

2.4 Experiment

In this study, we perform OSSEs comparing different global inversion setups using the same truth and a priori fluxes. The inversions system is run at a $6^\circ \times 4^\circ$ horizontal resolution and 25 vertical hybrid sigma-pressure levels from the surface to the top of the atmosphere. Simulations are performed for the period 1 June 2009 to 30 May 2010. The transport in TM5 is driven by meteorological fields from the European Centre for Medium-Range Weather Forecasts (ECMWF) ERA-interim reanalysis project (Dee et al., 2011). Table 2 provides an overview of the inversions that have been performed, specifying the fluxes that were optimized, the optimizer that was used with number of iterations, and the type of measurements assimilated. The PROXY inversion requires $X^{\text{model}}_{\text{CO2}}$ (see Eq. 1), which is calculated by sampling the output of a forward run of TM5 using posterior CO_2 fluxes from the SURFCO2 inversion and applying the GOSAT averaging kernel.

The TRU-DAT represents an inversion which assumes that we have perfect knowledge of $X^{\text{model}}_{\text{CO2}}$. It is used as a best-case scenario for the proxy method. In contrast, $X^{\text{model}}_{\text{CO2}}$ for PRICO2 was calculated using prior CO_2 fluxes transformed directly into observations using TM5 without optimization using CO_2 surface measurements. This inversion represents a worst case scenario for the proxy method. The RATIO inversion uses our new ratio method, assimilating surface CH_4 and CO_2 observations, and X_{ratio} for optimizing surface CH_4 and CO_2 fluxes. PROXY represents the common use of proxy retrievals in atmospheric inverse modelling. In PROXY, the same amount of measurements are assimilated in a series of two linear inversions: (1) optimization of CO_2 fluxes with surface observations (SURFCO2), (2) an inversion using surface CH_4 and $X^{\text{proxy}}_{\text{CH4}}$ (PROXY). We use 50 iterations of CONGRAD for both of these inversions. In RATIO, all the information is assimilated in a single inversion using 100 iteration of M1QN3.

2.5 Analysis

In Sect. 3, we analyze the monthly time series of posterior fluxes from different inversions using Taylor plots (Taylor, 2001) and mean annual departures from the true fluxes aggregated over the Transcom land regions. We only show the analysis of the fluxes over the land as the fluxes of CH_4 are negligible over the oceans. We define the following parameters to represent the average deviation of the posterior fluxes from the truth over all the Transcom land regions:

$$\begin{aligned}
&\kappa = \overline{|cor - 1|},\\
&\gamma = \overline{|\sigma/\sigma_{\text{truth}} - 1|},\\
&\beta = \overline{|bias|},
\end{aligned} \tag{4}$$

where *cor* is the cross-correlation between the posterior and true monthly flux time series for a Transcom region, and $\sigma/\sigma_{\text{truth}}$ is the relative SD of the posterior and true monthly flux time series of a Transcom region. In the Taylor plots, $\sigma/\sigma_{\text{truth}} = 1$ and *cor* = 1 represent the true fluxes and therefore, we subtract 1 from both the values in Eq. (4) to represent the deviation of prior or posterior fluxes from true fluxes. Finally, *bias* is the difference between the posterior and true net annual flux of a Transcom region. It should be noted that κ and γ are dimensionless, and β has a unit of $\mathrm{Tg\,yr^{-1}}$ for $\mathrm{CH_4}$ and $\mathrm{Pg\,C\,yr^{-1}}$ for $\mathrm{CO_2}$.Table 3 lists the values of these parameters for the inversions performed in this study. The closer these values are to zero for an inversion, the better it is performing, With each parameter at zero the agreement between the true and inversion-optimized fluxes is perfect.

3 Results

3.1 Ratio method implementation

Figure 3 summarizes the performance of RATIO (see also Table 2). The pseudo X_{ratio} measurements have typical values in the range of 4.4 to 4.8 $\mathrm{ppb\,ppm^{-1}}$. We observe that the latitudinal gradient of $\mathrm{CH_4}$ atmospheric concentration is a dominant mode of variation in X_{ratio}. The randomly generated globally and annually integrated a priori $\mathrm{CO_2}$ flux, combining land and ocean, is 2.01 $\mathrm{Pg\,C\,yr^{-1}}$ larger than the true flux (truth $= -4.65\,\mathrm{Pg\,C\,yr^{-1}}$, prior $= -2.640\,\mathrm{Pg\,C\,yr^{-1}}$). As a result of this, the a priori fluxes overestimate the global $\mathrm{CO_2}$ increase. The global annual prior $\mathrm{CH_4}$ flux is only 6.85 $\mathrm{Tg\,yr^{-1}}$ lower than the truth (truth = 541.764 $\mathrm{Tg\,yr^{-1}}$, prior = 534.905 $\mathrm{Tg\,yr^{-1}}$), which is a much smaller relative deviation from the true fluxes compared to $\mathrm{CO_2}$. Hence, the percentage mismatch between the modeled prior and measured X_{ratio} is mostly positive over the globe (Fig. 3c). The figure also compares the prior and posterior misfits of RATIO to the "true" X_{ratio}. The measurement uncertainty of X_{ratio} increases towards higher latitudes. We find a gradient norm reduction of ≈ 2000 for 100 iterations of M1QN3. As expected, the posterior mismatches are strongly reduced in comparioson to the prior, demonstrating that the ratio inversion system works mathematically and that it is reasonably efficient in minimizing the cost function. The improved fit of measurements also leads to a convergence of the posterior fluxes towards the true fluxes, as will be discussed in detail in Sects. 3.3 and 3.4.

3.2 TRU-DAT and PRICO2

As explained in Sect. 2.4, TRU-DAT and PRICO2 represent best and worst case scenarios of the impact of errors in $X_{\mathrm{CO2}}^{\text{model}}$ on the results of a proxy inversion. Here we analyze the differences between these inversions, which inform us about the sensitivity of the proxy method to errors in $X_{\mathrm{CO2}}^{\text{model}}$. Figure 4 compares the performance of PRICO2 and TRU-DAT using Taylor plots. In these plots, each point represents a 12 month timeseries of $\mathrm{CH_4}$ fluxes integrated over a Transcom land region. Compared to the prior ($\kappa = 0.286$ and $\gamma = 0.211$), the posterior fluxes of TRU-DAT shows much better agreement with the true fluxes ($\kappa = 0.024$ and $\gamma = 0.042$). PRICO2 ($\kappa = 0.210$ and $\gamma = 0.258$), on the other hand, performs even worse than the prior in terms of γ. Figure 5 shows how well the TRU-DAT and PRICO2 inversions are capable of reproducing the true annual fluxes integrated over Transcom land regions. The β values are 2.370, 2.409 and 0.621 $\mathrm{Tg\,yr^{-1}}$ for PRIOR, PRICO2 and TRU-DAT, respectively. Again, we observe that on average the results of TRU-DAT are closest to the truth, and that the results for PRICO2 are further away from truth than the a priori fluxes. This tells us that the performance of inversions assimilating proxy data is sensitive to our knowledge of the CO_2 fluxes. In practical applications, however, the CO_2 fluxes will first be optimized using surface measurements to obtain a better representation of atmospheric CO_2 concentrations. Inversions representing this approach will be discussed in the next section.

3.3 PROXY, RATIO and SURFCH4

Next we analyze the difference between the proxy inversion (PROXY), using optimized CO_2 concentrations from SURFCO2, and our new ratio method (RATIO). For comparison, we also include results of SURFCH4 using only surface CH_4 measurements. The performance of these inversions is analyzed as in Sect. 4.2, and the results are summarized in Figs. 6 and 7. All three inversions improve the *cor* of the posterior fluxes with the truth compared to the prior but have varied performance in improving $\sigma/\sigma_{\text{truth}}$. The prior fluxes of Boreal North America are closer to the truth than any of the posterior fluxes. However, it should be realized that the prior fluxes were created by adding random noise to the truth, which happens to be a small perturbation occasionally. This is why we average results over all Transcom land regions to derive meaningful comparisons. The κ and γ values, representing the average performance over Transcom land regions, are shown in Table 3. We observe that RATIO and PROXY perform better than SURFCH4, confirming the importance of information provided by the satellite measurements.

Figure 7 shows the departures of the annual fluxes from the truth aggregated over Transcom land regions. The β values are 2.37, 1.40, 1.43, and 1.96 $\mathrm{Tg\,yr^{-1}}$ for PRIOR, RATIO, PROXY and SURFCH4, respectively (see Table 3). Overall, we find that the performance of RATIO and PROXY is similar. RATIO performs better than PROXY in 6 regions, and PROXY is better in the other 5 regions. The PROXY inversion shows the worst performance in Boreal North America, Temperate North America and Boreal Eurasia, and RATIO has the worst performance in Southern Africa.

We find that with the additional information provided by the satellite measurements RATIO and PROXY are able to reproduce the true fluxes better than SURFCH4. However, it is difficult to conclude if RATIO or PROXY performs better, as their relative performances vary across the regions. As can be seen in Figs. 6 and 7, PROXY clearly has a poor performance over Temperate North America. Similarly, RATIO performs worse in Southern Africa than PROXY. These varying relative performances are further investigated in the next subsection. Annual flux uncertainties of the fluxes are shown as error bars in Fig. 7. It should be noted that unlike PROXY and SURFCH4, RA-

TIO does not estimate posterior uncertainties. This drawback of RATIO will be further discussed in Sect. 4. The reduction in uncertainty is larger for PROXY than SURFCH4 in the regions where we have less surface measurements (in Tropical South America, Temperate South America, Northern Africa). This can be attributed to the larger number of satellite observations in comparison to surface measurements in these regions. In other regions, both inversions show similar uncertainty reductions due to a higher gradient norm reduction achieved by SUFCH4 (3.1×10^{10}) compared to PROXY (3.9×10^{3}). Both inversions are run for 50 iterations, but PROXY has a larger number of data to assimilate than SURFCH4, and therefore, it achieves a lower gradient norm reduction.

3.4 $\mathbf{CO_2}$ fluxes

As explained in Sect. 1, the motivation for our ratio technique is to obtain a more consistent representation of the CO_2 concentration fields in the atmosphere. In this subsection, we address the question whether RATIO optimized CO_2 fluxes are indeed closer to the truth than those obtained using SURFCO2 (which are used for PROXY). Figure 8 shows the deviations of posterior CO_2 fluxes from the truth for RATIO and SURFCO2. In general, annual a priori CO_2 fluxes show large relative deviations from the truth compared to CH_4. This is a direct consequence of the assumed a priori flux uncertainties (see Table 1). The β values (Table 3) are 0.327, 0.185 and 0.134 $\mathrm{Pg\,C\,yr^{-1}}$ for PRIOR, SURFCO2 and RATIO, respectively. RATIO is able to constrain CO_2 fluxes better than SURFCO2. The difference between SURFCO2 and RATIO is explained by regions such as Temperate North America and Temperate South America, which are relatively poorly constrained by SURFCO2. In Temperate North America, due to coarse resolution of the model in combination with large emission gradients, large representation errors are assigned to the simulated measurements. Also, we do not take the full advantage of surface measurement coverage of this region as we use only fully processed NOAA/ESRL flask measurements. A lack of surface measurements can be the reason for poor performance of SURFCO2 in Temperate South America. We observe that RATIO is performing better in these regions with the help of satellite measurements.

Figure 9 shows how well the inversion-derived CO_2 fluxes reproduce the true seasonality. Compared with CH_4, the prior fluxes correlate well with the truth, despite their relatively large a priori uncertainties. This reflects the large seasonal variation in the biospheric CO_2 fluxes. For CO_2, the differences in the Taylor diagrams are dominated by variations in $\sigma/\sigma_{\text{truth}}$. Overall, RATIO ($\kappa = 0.125$, $\gamma = 0.225$) performs better than SURFCO2 ($\kappa = 0.180$, $\gamma = 0.241$). RATIO is able to reproduce the true seasonality for most regions except Northern Africa, Temperate Eurasia and Tropical Asia. In Temperate Eurasia, SURFCO2 performs very well. However, it performs worse than RATIO in Tropical Asia. In Tropical South America and Temperate South America, we find a similar performance of RATIO and SURFCO2. The prior for Europe does not deviate much from the truth, so the relative performance for the two methods cannot be judged adequately.

3.5 The link between $\mathrm{CO_2}$ and $\mathrm{CH_4}$

In principle, the performance of PROXY should improve with the performance of SURFCO2. If SURFCO2 reproduces the true $\mathrm{CO_2}$ fluxes exactly, the only source of error in $X_{\mathrm{CH4}}^{\mathrm{proxy}}$ due to $X_{\mathrm{CO2}}^{\mathrm{model}}$ will be the representation error of the finite resolution model used for generating spatio-temporal fields of $\mathrm{CO_2}$. Also in the case of RATIO, the correctness of posterior $\mathrm{CH_4}$ fluxes is dependent upon the correctness of $\mathrm{CO_2}$ fluxes and vice-versa. For example, Figs. 8 and 9 show that Southern Africa has a poor performance of RATIO, and that SURFCO2 has a poor performance in Temperate North America for constraining $\mathrm{CO_2}$ fluxes. This is also reflected in the poor performance of RATIO and PROXY in constraining $\mathrm{CH_4}$ fluxes in these regions (Sect. 3.3). The performance of SURFCO2 varies regionally, which causes a corresponding pattern in the performance of PROXY. The same relation should hold for the posterior $\mathrm{CO_2}$ and $\mathrm{CH_4}$ fluxes calculated with RATIO. To quantify this relation, we define $\boldsymbol{p}_{\mathrm{CH_4}}$ as a measure of the relative accuracy of RATIO and PROXY derived $\mathrm{CH_4}$ fluxes, and $\boldsymbol{p}_{\mathrm{CO_2}}$ as a measure of the relative accuracy of RATIO and SURFCO2 derived biosphere $\mathrm{CO_2}$ fluxes for each Transcom region. They are defined as

$$
\begin{aligned}
\boldsymbol{p}_{\mathrm{CH4}} &= \left|\boldsymbol{x}_{\mathrm{CH4}}^{\mathrm{PROXY}} - \boldsymbol{x}_{\mathrm{CH4}}^{\mathrm{truth}}\right| - \left|\boldsymbol{x}_{\mathrm{CH4}}^{\mathrm{RATIO}} - \boldsymbol{x}_{\mathrm{CH4}}^{\mathrm{truth}}\right|, \\
\boldsymbol{p}_{\mathrm{CO2}} &= \left|\boldsymbol{x}_{\mathrm{CO2}}^{\mathrm{SURFCO2}} - \boldsymbol{x}_{\mathrm{CO2}}^{\mathrm{truth}}\right| - \left|\boldsymbol{x}_{\mathrm{CO2}}^{\mathrm{RATIO}} - \boldsymbol{x}_{\mathrm{CO2}}^{\mathrm{truth}}\right|,
\end{aligned}
\tag{5}
$$

where the x's denote timeseries of monthly fluxes integrated over land Transcom regions. The subscripts indicate the tracer, and the superscripts indicate whether the fluxes refer to the truth or inversion estimates. $\boldsymbol{p}_{\mathrm{CH4}}$ and $\boldsymbol{p}_{\mathrm{CO2}}$ are arrays of 12 month timeseries for each Transcom land region. They are defined such that: (1) $\boldsymbol{p}_{\mathrm{CH4},i} > 0$ implies that RATIO is performing better than PROXY for $\mathrm{CH_4}$ fluxes in the month i. (2) $\boldsymbol{p}_{\mathrm{CO2},i} > 0$ implies that RATIO is performing better than SURFCO2 for $\mathrm{CO_2}$ fluxes in month i. (3) For values of $\boldsymbol{p}_{\mathrm{CH4},i}$ and $\boldsymbol{p}_{\mathrm{CO2},i}$ less than 0 the reverse of (1) and (2) is true.

The upper panel of Fig. 10 shows $\boldsymbol{p}_{\mathrm{CO2}}$ and $\boldsymbol{p}_{\mathrm{CH4}}$ series for Boreal North America. Lower panel of Fig. 10 shows the cross-correlations between $\boldsymbol{p}_{\mathrm{CH4}}$ and $\boldsymbol{p}_{\mathrm{CO2}}$ for each Transcom land region. As it can be seen, this value is above 0.7 (mean = 0.809) for all regions except for Australia (0.202) and Boreal Eurasia (0.539). A lack of surface measurements in these two regions can be the reason for the low correlation, as surface measurement stations are needed for good performance of both RATIO and PROXY (Sect. 4). Overall, we conclude that the relative performance of the proxy and ratio methods depends strongly on the relative performance of the surface-only and ratio $\mathrm{CO_2}$ inversions.

4 Discussion

We have developed the "ratio" method for TM5-4DVAR inversions system. It is an inversion system for assimilating the ratio of satellite-retrieved total columns of $\mathrm{CH_4}$ and $\mathrm{CO_2}$ along with surface measurements for constraining their surface fluxes. The main advantage of this method over the traditional proxy method is that it does not impose model-derived CO_2 concentrations as a hard constraint on the CH_4 flux optimization. Instead, our method allows optimization of CO_2 and CH_4 fluxes within a single consistent framework. This way we can benefit from the proxy retrieval, which has proven to be highly efficient in reducing the errors due to light-path modification by atmospheric scattering, but at the same time, avoid projection of errors in $X_{\mathrm{CO2}}^{\mathrm{model}}$ on the inverted CH_4 fluxes. The method requires assimilation of surface measurements of CH_4 and CO_2 as an additional constraint, since a ratio alone is not a sufficient constraint for absolute values of CH_4 and CO_2 fluxes. For example, the inversions can reduce the absolute CH_4 and CO_2 modeled columns by the same factor and can still fit their ratio column to give a lower value of the cost function (Eq. 3).

The performance of the ratio method is tested in comparison with the traditional proxy method and surface-only inversions in an OSSE using the TM5-4DVAR atmospheric inversion system. Overall, we observe that the ratio method is capable of reproducing the true CH_4 and CO_2 fluxes better than the surface-only inversion. The performance of the ratio method in comparison to the proxy method varies among Transcom land regions. The performance of inversions assimilating satellite data in this study is optimistic compared to inversions using real observations as we have not introduced any systematic biases in our measurements. Also, as we do not filterout measurements taken in cloudy scenes and we use medium gain measurements in our inversion, we are optimistic about the satellite coverage in the tropics compared to real-life inversions. However, it is also true that satellite measurements are an important additional source of information about GHGs concentrations in these regions.

The ratio method is a more complicated inversion to solve than a proxy inversion as it is a non-linear inversion problem, and therefore the widely used CONGRAD optimizer cannot be used. In our setup, we use the M1QN3 optimizer, which is capable of handling the non-linearty. However, to inter-compare inversions using different optimizers requires attention as mathematically their mode of operation is different. For example, CONGRAD solves for the largest spatial and temporal scales in the first few iterations, gradually adjusting finer scales in subsequent iterations. M1QN3 works in similar manner, however, it has a much slower convergence rate for the finer scales than CONGRAD. Hence the overall convergence rate of M1QN3 is slower than CONGRAD, and to achieve the same gradient norm reduction it takes more iterations (Krol et al., 2013).

Another drawback of M1QN3 compared to CONGRAD is that no information is obtained about posterior flux uncertainties. They are essential for inverse modeling applications using real data to quantify the constraints on the fluxes imposed by measurements. This is true, despite the fact that several important sources of uncertainty, such as transport model uncertainties, are difficult to account for. Furthermore, the accuracy of CONGRAD's uncertainty approximation may be rather poor for large optimization problems, limiting its use. An alternative method for calculating posterior uncertainties is to use a Monte Carlo approach (Chevallier et al., 2007). This method can be applied also to inversions using M1QN3, although the method is computationally expensive. So far we have not investigated possible alternatives for M1QN3. However, we would like to stress that there is a scope to find a more efficient optimizer for solving this non-linear optimization problem, and future studies into the application of the ratio method should put an effort in this direction.

Fraser et al. (2014) developed a method for assimilating X_{ratio} in the MAP inversion setup coupled to the GEOS-Chem global 3-D atmospheric chemistry transport model. Similar to our findings, their OSSEs show that the assimilation of X_{ratio} along with surface measurements of CH4 and CO2 can reproduce the true fluxes. However, there are some important differences with our study:

1. We focus on a comparison between the proxy and ratio approach and also perform a CO_2 inversion using surface measurements for calculating the model derived CO_2 fields used in the proxy approach. This way the propagation of errors from modeled CO_2 fields into proxy CH_4 measurements is also simulated. Instead, Fraser et al. (2014) add a constant or random bias to the X_{ratio} measurements.

2. Fraser et al. (2014) report posterior uncertainties of CH_4 and CO_2 fluxes derived from their X_{ratio} inversions. Although posterior flux uncertainties can in principle be derived from our method also, they are not reported here for computational reasons.

3. The ratio inversion system is weakly non-linear. The Fraser et al. (2014) ratio inversions assume linearity. We do a non-linear inversion using a suitable optimizer.

Now that we have demonstrated that the ratio method works in a synthetic environment, the next step is the application of the method to real satellite data. A first step in this direction is to validate GOSAT observed X_{CH4}: X_{CO2} with TCCON. After that we plan to apply the ratio method to real satellite data, and compare the outcome with inversions using the GOSAT proxy and full-physics retrieval products. With improved constraints on the CO_2 side of the problem, as more space borne CO_2 measurements becoming available from GOSAT and OCO-2, the proxy method is expected to perform better for methane. In this case one would expect the results of the proxy and ratio methods to converge. Whether or not this will really happen depends on the mutual consistency of the various data streams. The ratio method provides an internally consistent setup (i.e within a single inversion system) to test this and to identify remaining biases. It should be noted that computationally, the ratio method has the advantage that it optimizes CH_4 and CO_2 fluxes together. This method can also be applied to other pairs of tracers, which are retrieved from close-by spectral ranges in the satellite measurement spectra. For example, CO total columns will be retrieved from TROPOMI (to be launched in 2016) using CH_4 as the proxy for atmospheric scattering, and there is a possibility that our ratio method can be applied successfully to this pair of tracers.

5 Conclusions

We developed a new inverse modeling method within the TM5-4DVAR inverse modeling framework for direct assimilation of satellite observed ratios of total column CH_4 and CO_2. The dual tracer inversion solves for surface fluxes of CH_4 and CO_2. Our current implementation also assimilates surface measurements of CO_2 and CH_4 to further constrain the two tracer inverse problem. To deal with the weak non-linearity introduced by the optimization of tracer ratios we make use of the M1QN3 optimizer, instead of the CONGRAD optimizer, which was used so far for inversions using proxy retrievals. Although the optimization of the ratio inversion using M1QN3 is about a factor of 2 less efficient than the corresponding proxy inversion using CONGRAD, we nevertheless find satisfactory gradient norm reductions (by a factor of ≈ 2000 in 100 iterations). We tested our method in an OSSE setup. We observe good convergence of posterior model columns toward the true ratio columns, and the ratio method is able to reproduce the true CH_4 and CO_2 fluxes from randomly perturbed prior fluxes.

We performed additional inversions in our OSSE setup to compare the performance of inversions using proxy and ratio retrievals from GOSAT. In addition, we compare the performances of these inversions, which also use surface measurements, with inversions that only use surface measurements. Additional inversions are performed to test the sensitivity of proxy inversions to the quality of the model derived CO_2 concentrations, which are used to translate the retrieved tracer ratios into total columns of CH_4. The performance of these inversions is evaluated by comparing the inversion-derived fluxes to a set of true fluxes from which the synthetic measurements were derived. The performance is assessed for monthly and annual fluxes integrated over the 11 Transcom land regions. Our results demonstrate that the estimation of CH_4 fluxes using the proxy inversion is sensitive to errors in the modeled derived CO_2 concentrations.

We conclude that for most Transcom regions the ratio method is capable of reproducing the true seasonality and annually integrated CH_4 fluxes. However, it should be noted that availability of surface measurements is important for good performance of the ratio method. The relative performance of the proxy and ratio methods shows a relationship with errors in CO_2, with ratio method performing better in regions where the CO_2 fluxes are poorly constrained. In our synthetic simulations, the ratio inversion is capable of improving the CO_2 fluxes compared with the use of CO_2 surface-only measurements, which explains why it outperforms the proxy method in certain regions. This points to the applicability of the ratio method for improving CO_2 fluxes in these regions. Further research is needed to test the performance of the ratio method in applications using real satellite data.

Appendix A: M1QN3 and CONGRAD

We tested the convergence rate of CONGRAD and M1QN3 using the setup of PROXY described in section 2.4. For this purpose, we carried out inversions with both optimizers for 30, 60 and 100 iterations and compared these to the standard inversion using 50 iterations. Figure 1.11 shows the corresponding posterior CH_4 flux departures from PROXY that are also shown in figure 7. We find that both the optimizers converge within 100 iterations. After 60 iterations, CONGRAD already reaches the solution, whereas M1QN3 shows slower convergence. Significant flux differences are found between the optimizers for inversions with 30 and 60 iterations. For CONGRAD, the difference between inversions with 50 and 60 iterations is negligible.

Acknowledgements. This work is supported by the Netherlands Organization for Scientific Research (NWO), project number ALW-GO-AO/11-24. The computations were carried out on the Dutch national supercomputer Cartesius, and we thank SURFSara (www.surfsara.nl) for their support. We thank our data providers: NOAA/ESRL cooperative flask-sampling network surface observations were obtained from the website http://www.esrl.noaa.gov/gmd/dv/ftpdata.html; Access to the GOSAT data was granted through the 3rd GOSAT research announcement jointly issued by JAVA, NIES, and MOE. We would like to acknowledge Guillaume Monteil (IMAU) for his useful input.

References

Alexe, M., Bergamaschi, P., Segers, A., Detmers, R., Butz, A., Hasekamp, O., Guerlet, S., Parker, R., Boesch, H., Frankenberg, C., Scheepmaker, R. A., Dlugokencky, E., Sweeney, C., Wofsy, S. C., and Kort, E. A.: Inverse modelling of CH_4 emissions for 2010–2011 using different satellite retrieval products from GOSAT and SCIAMACHY, Atmos. Chem. Phys., 15, 113–133, doi:10.5194/acp-15-113-2015, 2015.

Basu, S., Guerlet, S., Butz, A., Houweling, S., Hasekamp, O., Aben, I., Krummel, P., Steele, P., Langenfelds, R., Torn, M., Biraud, S., Stephens, B., Andrews, A., and Worthy, D.: Global CO_2 fluxes estimated from GOSAT retrievals of total column CO_2, Atmos. Chem. Phys., 13, 8695–8717, doi:10.5194/acp-13-8695-2013, 2013.

Basu, S., Krol, M., Butz, A., Clerbaux, C., Sawa, Y., Machida, T., Matsueda, H., Frankenberg, C., Hasekamp, O., and Aben, I.: The seasonal variation of the CO_2 flux over Tropical Asia estimated from GOSAT, CONTRAIL, and IASI, Geophys. Res. Lett., 41, 1809–1815, doi:10.1002/2013GL059105, 2014.

Bergamaschi, P. and Frankenberg, C.: Inverse modeling of global and regional CH_4 emissions using SCIAMACHY satellite retrievals, J. Geophys. Res., 114, 1–28, doi:10.1029/2009JD012287, 2009.

Bergamaschi, P., Frankenberg, C., Meirink, J. F., Krol, M., Dentener, F., Wagner, T., Platt, U., Kaplan, J. O., Körner, S., Heimann, M., Dlugokencky, E. J., and Goede, A.: Satellite chartography of atmospheric methane from SCIAMACHY on board ENVISAT: 2. Evaluation based on inverse model simulations, J. Geophys. Res., 112, D02304, doi:10.1029/2006JD007268, 2007.

Bousquet, P., Ciais, P., Miller, J. B., Dlugokencky, E. J., Hauglustaine, D. a., Prigent, C., Van der Werf, G. R., Peylin, P., Brunke, E.-G., Carouge, C., Langenfelds, R. L., Lathière, J., Papa, F., Ramonet, M., Schmidt, M., Steele, L. P., Tyler, S. C., and White, J.: Contribution of anthropogenic and natural sources to atmospheric methane variability, Nature, 443, 439–43, doi:10.1038/nature05132, 2006.

Bousquet, P., Ringeval, B., Pison, I., Dlugokencky, E. J., Brunke, E.-G., Carouge, C., Chevallier, F., Fortems-Cheiney, A., Frankenberg, C., Hauglustaine, D. A., Krummel, P. B., Langenfelds, R. L., Ramonet, M., Schmidt, M., Steele, L. P., Szopa, S., Yver, C., Viovy, N., and Ciais, P.: Source attribution of the changes in atmospheric methane for 2006–2008, Atmos. Chem. Phys., 11, 3689–3700, doi:10.5194/acp-11-3689-2011, 2011.

Chevallier, F., Bréon, F.-M., and Rayner, P. J.: Contribution of the Orbiting Carbon Observatory to the estimation of CO_2 sources and sinks: Theoretical study in a variational data assimilation framework, J. Geophys. Res., 112, D09307, doi:10.1029/2006JD007375, 2007.

Cressot, C., Chevallier, F., Bousquet, P., Crevoisier, C., Dlugokencky, E. J., Fortems-Cheiney, A., Frankenberg, C., Parker, R., Pison, I., Scheepmaker, R. A., Montzka, S. A., Krummel, P. B., Steele, L. P., and Langenfelds, R. L.: On the consistency between global and regional methane emissions inferred from SCIAMACHY, TANSO-FTS, IASI and surface measurements, Atmos. Chem. Phys., 14, 577–592, doi:10.5194/acp-14-577-2014, 2014.

Dee, D. P., Uppala, S. M., Simmons, A. J., Berrisford, P., Poli, P., Kobayashi, S., Andrae, U., Balmaseda, M. A., Balsamo, G., Bauer, P., Bechtold, P., Beljaars, A. C. M., van de Berg, L., Bidlot, J., Bormann, N., Delsol, C., Dragani, R., Fuentes, M., Geer, A. J., Haimberger, L., Healy, S. B., Hersbach, H., Hólm, E. V., Isaksen, L., Kållberg, P., Köhler, M., Matricardi, M., McNally, A. P., Monge-Sanz, B. M., Morcrette, J.-J., Park, B.-K., Peubey, C., de Rosnay, P., Tavolato, C., Thépaut, J.-N., and Vitart, F.: The ERA-Interim reanalysis: configuration and performance of the data assimilation system, Q. J. Roy. Meteor. Soc., 137, 553–597, doi:10.1002/qj.828, 2011.

Dlugokencky, E. J., Bruhwiler, L., White, J. W. C., Emmons, L. K., Novelli, P. C., Montzka, S. A., Masarie, K. A., Lang, P. M., Crotwell, A. M., Miller, J. B., and Gatti, L. V.: Observational constraints on recent increases in the atmospheric CH_4 burden, Geophys. Res. Lett., 36, L18803, doi:10.1029/2009GL039780, 2009.

Errico, R. M.: What is an adjoint model?, B. Am. Meteorol. Soc., 78, 2577–2591, doi:10.1175/1520-0477(1997)078<2577:WIAAM>2.0.CO;2, 1997.

Ferretti, D. F., Miller, J. B., White, J. W. C., Etheridge, D. M., Lassey, K. R., Lowe, D. C., Macfarling Meure, C. M., Dreier, M. F., Trudinger, C. M., van Ommen, T. D., and Langenfelds, R. L.: Unexpected changes to the global methane budget over the past 2000 years, Science, 309, 1714–1717, doi:10.1126/science.1115193, 2005.

Frankenberg, C., Meirink, J. F., van Weele, M., Platt, U., and Wagner, T.: Assessing methane emissions from global space-borne observations, Science, 308, 1010–1014, doi:10.1126/science.1106644, 2005.

Fraser, A., Palmer, P. I., Feng, L., Boesch, H., Cogan, A., Parker, R., Dlugokencky, E. J., Fraser, P. J., Krummel, P. B., Langenfelds, R. L., O'Doherty, S., Prinn, R. G., Steele, L. P., van der Schoot, M., and Weiss, R. F.: Estimating regional methane surface fluxes: the relative importance of surface and GOSAT mole fraction measurements, Atmos. Chem. Phys., 13, 5697–5713, doi:10.5194/acp-13-5697-2013, 2013.

Fraser, A., Palmer, P. I., Feng, L., Bösch, H., Parker, R., Dlugokencky, E. J., Krummel, P. B., and Langenfelds, R. L.: Estimating regional fluxes of CO_2 and CH_4 using space-borne observations of XCH_4: XCO_2, Atmos. Chem. Phys., 14, 12883–12895, doi:10.5194/acp-14-12883-2014, 2014.

Gilbert, J. C. and Lemaréchal, C.: Some numerical experiments with variable-storage quasi-Newton algorithms, Math. Program., 45, 407–435, doi:10.1007/BF01589113, 1989.

Gurney, K., Law, R., Denning, A., Rayner, P., Baker, D., Bousquet, P., Bruhwiler, L., Chen, H., Ciais, P., Fan, S., Fung, I., Gloor, M., Heimann, M., Higuchi, K., John, J., Maki, T., Maksyutov, S., Ken, M., Peylin, P., Prather, M., Pak, B. C., Randerson, J., Sarmiento, J., Taguchi, S., Takahashi, T., and Yuen, C.-W.: Towards robust regional estimates of CO2 sources and sinks using atmospheric transport models, Nature, 415, 626–630, doi:10.1038/415626a, 2002.

Hein, R., Crutzen, P. J., and Heimann, M.: An inverse modeling approach to investigate the global atmospheric methane cycle, Global Biogeochem. Cy., 11, 43–76, doi:10.1029/96GB03043, 1997.

Houweling, S., Kaminski, T., Dentener, F., Lelieveld, J., and Heimann, M.: Inverse modeling of methane sources and sinks using the adjoint of a global transport model Sander global methane emissions, J. Geophys. Res., 104, 26137–26160, 1999.

Houweling, S., Krol, M., Bergamaschi, P., Frankenberg, C., Dlugokencky, E. J., Morino, I., Notholt, J., Sherlock, V., Wunch, D., Beck, V., Gerbig, C., Chen, H., Kort, E. A., Röckmann, T., and Aben, I.: A multi-year methane inversion using SCIAMACHY, accounting for systematic errors using TCCON measurements, Atmos. Chem. Phys., 14, 3991–4012, doi:10.5194/acp-14-3991-2014, 2014.

Kirschke, S., Bousquet, P., Ciais, P., Saunois, M., Canadell, J. G., Dlugokencky, E. J., Bergamaschi, P., Bergmann, D., Blake, D. R., Bruhwiler, L., Cameron-Smith, P., Castaldi, S., Chevallier, F., Feng, L., Fraser, A., Heimann, M., Hodson, E. L., Houweling, S., Josse, B., Fraser, P. J., Krummel, P. B., Lamarque, J.-F., Langenfelds, R. L., Le Quéré, C., Naik, V., O'Doherty, S., Palmer, P. I., Pison, I., Plummer, D., Poulter, B., Prinn, R. G., Rigby, M., Ringeval, B., Santini, M., Schmidt, M., Shindell, D. T., Simpson, I. J., Spahni, R., Steele, L. P., Strode, S. A., Sudo, K., Szopa, S., van der Werf, G. R., Voulgarakis, A., van Weele, M., Weiss, R. F., Williams, J. E., and Zeng, G.: Three decades of global methane sources and sinks, Nat. Geosci., 6, 813–823, doi:10.1038/ngeo1955, 2013.

Krol, M., Houweling, S., Bregman, B., van den Broek, M., Segers, A., van Velthoven, P., Peters, W., Dentener, F., and Bergamaschi, P.: The two-way nested global chemistry-transport zoom model TM5: algorithm and applications, Atmos. Chem. Phys., 5, 417–432, doi:10.5194/acp-5-417-2005, 2005.

Krol, M. C., Hooghiemstra, P. B., van Leeuwen, T. T., van der Werf, G. R., Novelli, P. C., Deeter, M. N., Aben, I., and Röckmann, T.: Correction to "Interannual variability of carbon monoxide emission estimates over South America from 2006 to 2010", J. Geophys. Res.-Atmos., 118, 5061–5064, doi:10.1002/jgrd.50389, 2013.

Kuze, A., Suto, H., Nakajima, M., and Hamazaki, T.: Thermal and near infrared sensor for carbon observation Fourier-transform spectrometer on the Greenhouse Gases Observing Satellite for greenhouse gases monitoring, Appl. Optics, 48, 6716–6733, 2009.

Lanczos, C.: An iteration method for the solution of the eigenvalue problem of linear differential and integral operators, J. Res. Nat. Bur. Stand., 45, 255, doi:10.6028/jres.045.026, 1950.

Meirink, J. F., Bergamaschi, P., and Krol, M. C.: Four-dimensional variational data assimilation for inverse modelling of atmospheric methane emissions: method and comparison with synthesis inversion, Atmos. Chem. Phys., 8, 6341–6353, doi:10.5194/acp-8-6341-2008, 2008.

Monteil, G., Houweling, S., Dlugockenky, E. J., Maenhout, G., Vaughn, B. H., White, J. W. C., and Rockmann, T.: Interpreting methane variations in the past two decades using measurements of CH_4 mixing ratio and isotopic composition, Atmos. Chem. Phys., 11, 9141–9153, doi:10.5194/acp-11-9141-2011, 2011.

Monteil, G., Houweling, S., Butz, A., Guerlet, S., Schepers, D., Hasekamp, O., Frankenberg, C., Scheepmaker, R., Aben, I., and Röckmann, T.: Comparison of CH_4 inversions based on 15 months of GOSAT and SCIAMACHY observations, J. Geophys. Res.-Atmos., 118, 11807–11823, doi:10.1002/2013JD019760, 2013.

Müller, J.-F. and Stavrakou, T.: Inversion of CO and NO_x emissions using the adjoint of the IMAGES model, Atmos. Chem. Phys., 5, 1157–1186, doi:10.5194/acp-5-1157-2005, 2005.

Myhre, G., Shindell, D., Bréon, F.-M., Collins, W., Fuglestvedt, J., Huang, J., Koch, D., Lamarque, J.-F., Lee, D., Mendoza, B., Nakajima, T., Robock, A., Stephens, G., Takemura, T., and Zhang, H.: Anthropogenic and Natural Radiative Forcing, in: Climate Change 2013: The Physical Science Basis. Contribution of Working Group I to the Fifth Assessment Report of the Intergovernmental Panel on Climate Change, Cambridge University Press, Cambridge, UK and New York, NY, USA, 2013.

Nisbet, E. G., Dlugokencky, E. J., and Bousquet, P.: Methane on the rise–again, Science, 343, 493–495, doi:10.1126/science.1247828, 2014.

Peters, W., Jacobson, A. R., Sweeney, C., Andrews, A. E., Conway, T. J., Masarie, K., Miller, J. B., Bruhwiler, L. M. P., Pétron, G., Hirsch, A. I., Worthy, D. E. J., van der Werf, G. R., Randerson, J. T., Wennberg, P. O., Krol, M. C., and Tans, P. P.: An atmospheric perspective on North American carbon dioxide exchange: CarbonTracker, P. Natl. Acad. Sci. USA, 104, 18925–18930, doi:10.1073/pnas.0708986104, 2007.

Table 1. Covariance parameters of the a priori flux uncertainties per grid box per month used in the inversions. The uncertainty is expressed as a fraction of the a priori flux. Error correlations are defined by exponential ("e") and Gaussian ("g") correlation functions using the specified length scales (Basu et al., 2013).

Tracer category	Uncertainty (%)	Temporal (months)	Spatial (km)
CH_4 Total	50	3.0-e	500.0-g
CO_2 Biosphere	250	3.0-e	1000.0-g
CO_2 Ocean	250	6.0-e	1000.0-g

Table 2. Summary of the inversions performed in this study.

Inversion	Measurements	Fluxes optimized	Optimizer (No of iterations)
RATIO	X_{ratio}, surface CH_4, CO_2	CH_4, CO_2	M1QN3 (100)
SURFCO2	surface CO_2	CO_2	CONGRAD (50)
PROXY	$X^{\mathrm{proxy}}_{\mathrm{CH4}}$, surface CH_4	CH_4	CONGRAD (50)
SURFCH4	surface CH_4	CH_4	CONGRAD (50)
TRU-DAT	$X^{\mathrm{proxy}}_{\mathrm{CH4}}$, surface CH_4	CH_4	CONGRAD (50)
PRICO2	$X^{\mathrm{proxy}}_{\mathrm{CH4}}$, surface CH_4	CH_4	CONGRAD (50)

Schepers, D., Guerlet, S., Butz, A., Landgraf, J., Frankenberg, C., Hasekamp, O., Blavier, J.-F., Deutscher, N. M., Griffith, D. W. T., Hase, F., Kyro, E., Morino, I., Sherlock, V., Sussmann, R., and Aben, I.: Methane retrievals from Greenhouse Gases Observing Satellite (GOSAT) shortwave infrared measurements: Performance comparison of proxy and physics retrieval algorithms, J. Geophys. Res., 117, D10307, doi:10.1029/2012JD017549, 2012.

Spahni, R., Chappellaz, J., Stocker, T. F., Loulergue, L., Hausammann, G., Kawamura, K., Flückiger, J., Schwander, J., Raynaud, D., Masson-Delmotte, V., and Jouzel, J.: Atmospheric methane and nitrous oxide of the Late Pleistocene from Antarctic ice cores, Science, 310, 1317–1321, doi:10.1126/science.1120132, 2005.

Taylor, K. E.: Summarizing multiple aspects of model performance in a single diagram, J. Geophys. Res., 106, 7183–7192, 2001.

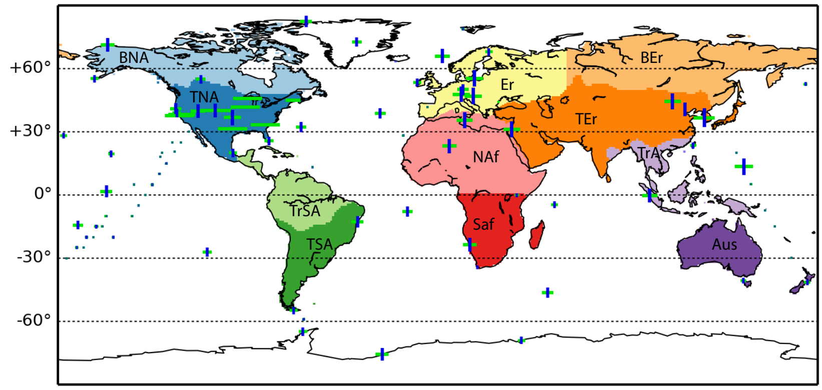

Figure 1. The dynamic symbols (blue-green crosses) show the location of the NOAA measurements sites included in inversions using surface measurements (see Table 2). The lengths of vertical blue and horizontal green bars are proportional to the number of CO_2 and CH_4 measurements, respectively. Continents are divided into 11 Transcom land regions (Gurney et al., 2002) which will be referred to in Sects. 4 and 3 as: Boreal North America (BNA), Temperate North America (TNA), Tropical South America (TrSA), Temperate South America (TSA), Northern Africa (NAf), Southern Africa (SAf), Boreal Eurasia (BEr), Temperate Eurasia (TEr), Tropical Asia (TrAs), Australia (Aus), and Europe (Eur).

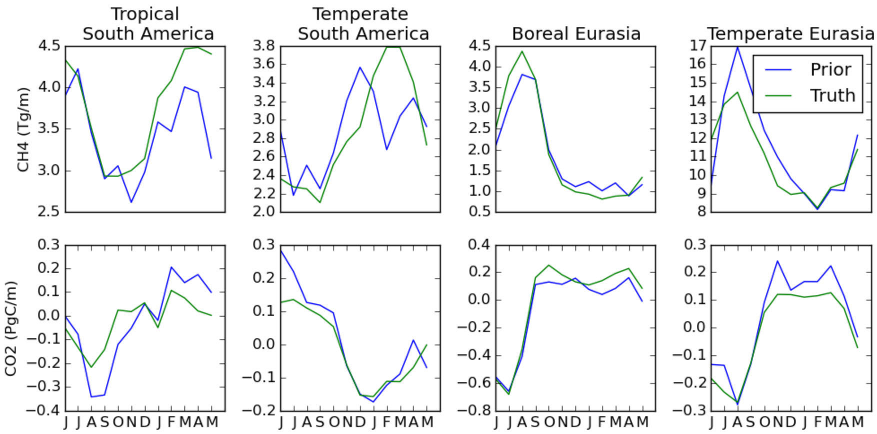

Figure 2. Timeseries of the true (green) and prior (blue) fluxes integrated over Tropical South America, Temperate South America, Boreal Eurasia and Temperate Eurasia. For CH_4, we show the total fluxes, and for CO_2, we show the biosphere fluxes. (see Table 1)

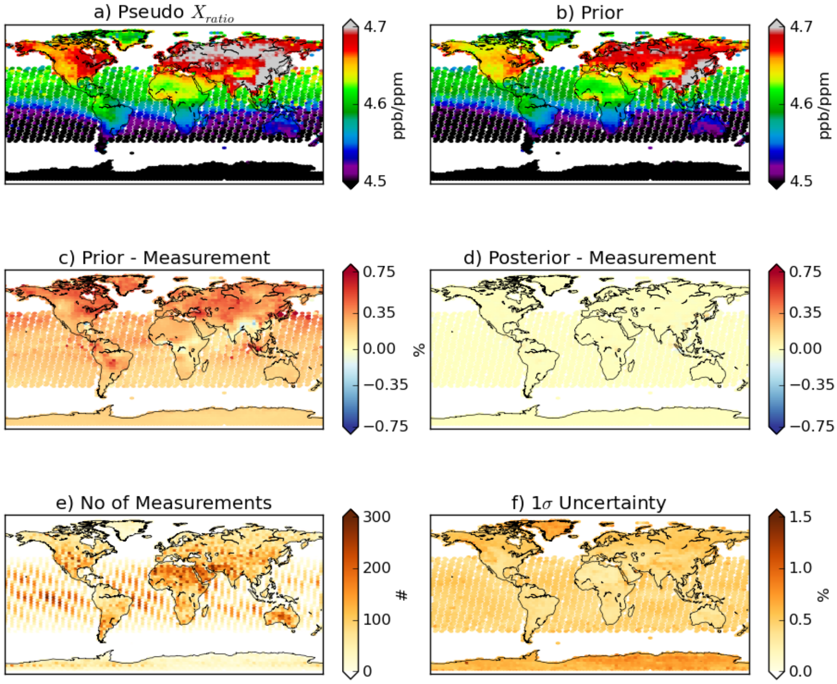

Figure 3. Fit of the RATIO inversion to the annually averaged "true" X_{ratio} pseudo measurements. **(a)** True pseudo X_{ratio} measurement, **(b)** a priori modeled X_{ratio}, **(c)** mismatch between the a priori model and the pseudo data, **(d)** the corresponding mismatch of the posterior model, **(e)** the number of GOSAT measurements, **(f)** the 1σ data uncertainty of X_{ratio}. The values represent yearly averages per $6^\circ \times 4^\circ$ (latitude $\times$ longitude) grid box, except the bottom left panel which shows yearly integrals on $6^\circ \times 4^\circ$ (latitude $\times$ longitude).

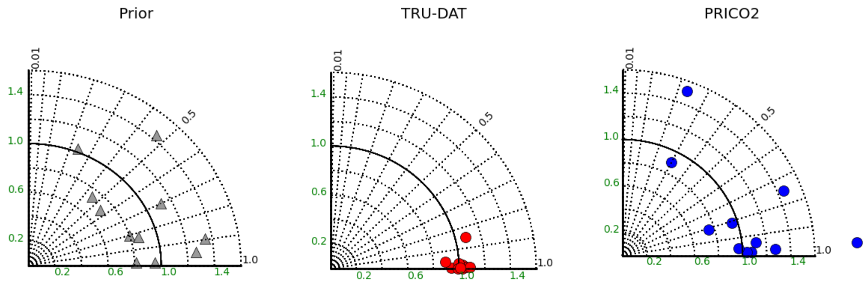

Figure 4. Taylor plots (Taylor, 2001) of monthly prior (grey triangles) and posterior CH_4 fluxes integrated over 11 Transcom land regions for the inversions TRU-DAT (red circles) and PRICO2 (blue circles). In these plots, each dot represents a seasonal variation of a single Transcom region. The true fluxes are at the intersection point of the x axis and the bold arc (representing a $cor = 1$ and $\sigma/\sigma_{\text{truth}} = 1$).

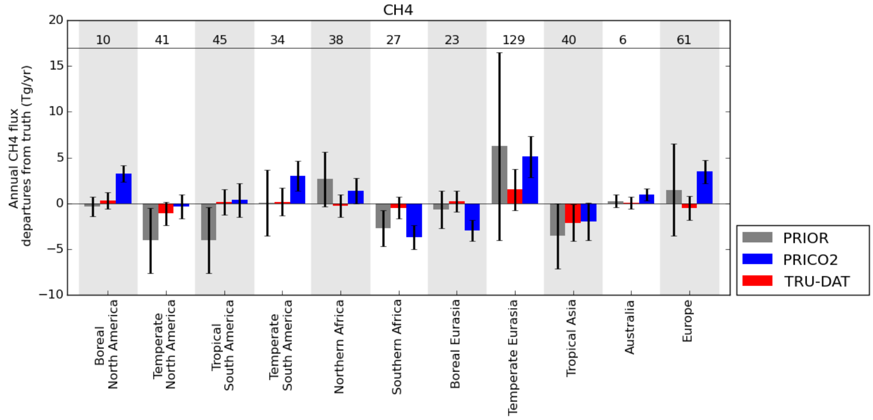

Figure 5. Annual prior and posterior CH_4 flux departures from the true fluxes for the Transcom land regions for the inversions TRU-DAT and PRICO2. The true fluxes are written at the top of the plot in $\mathrm{Tg\,yr^{-1}}$. The vertical black lines on the bars show 1σ uncertainty of the corresponding values.

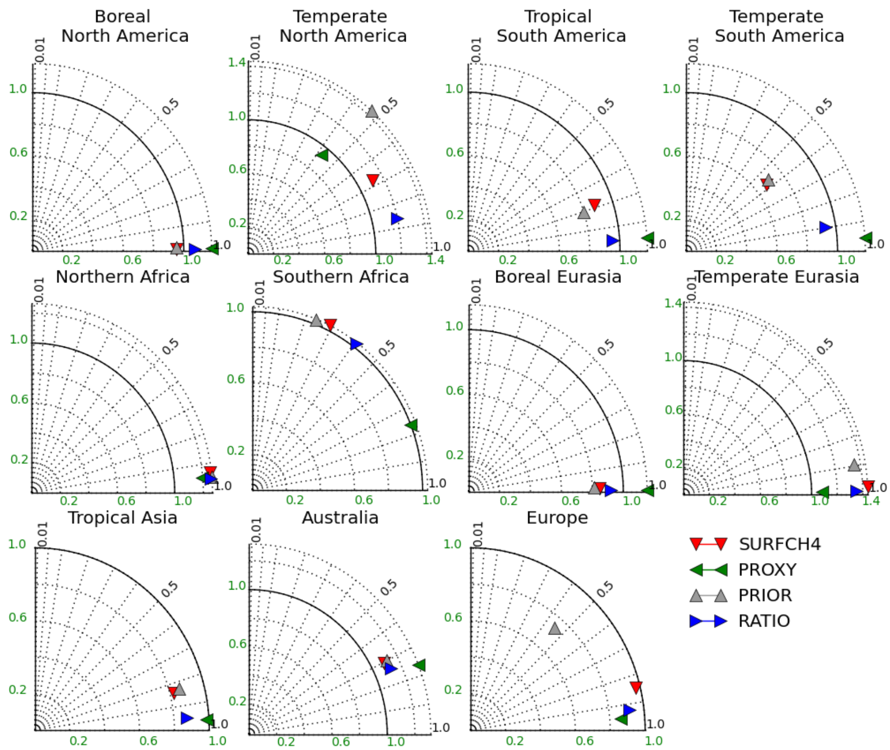

Figure 6. As Fig. 4 for the RATIO, PROXY and SURFCH4 inversions.

Table 3. κ, γ and β values of the inversions performed in this study (see Eq. 4 and Table 2). The β values have a unit of $\mathrm{Tg\,yr^{-1}}$ for CH_4 and $\mathrm{Pg\,C\,yr^{-1}}$ for CO_2. κ and γ are unitless quantities.

Tracer	Inversion	κ	γ	β
CH_4				
	PRIOR	0.286	0.211	2.370
	RATIO	0.122	0.129	1.396
	PROXY	0.119	0.137	1.432
	SURFCH4	0.218	0.162	1.959
	TRU-DAT	0.024	0.042	0.621
	PRICO2	0.210	0.258	2.409
CO_2				
	PRIOR	0.232	0.392	0.327
	SURFCO2	0.180	0.241	0.185
	RATIO	0.125	0.225	0.134

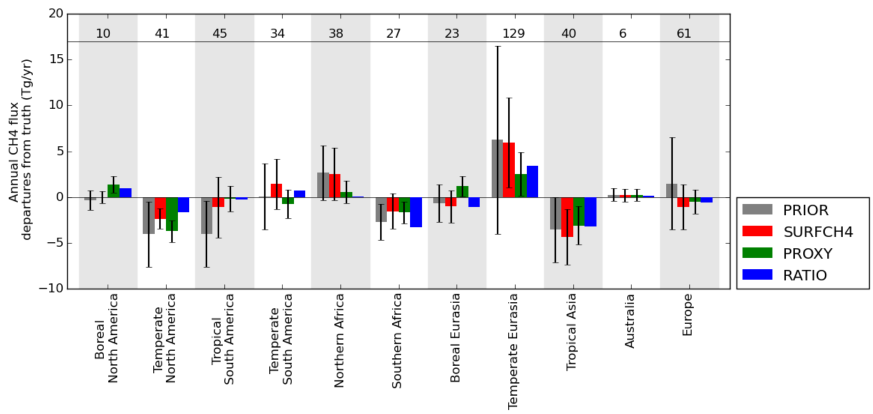

Figure 7. As Fig. 5 for RATIO, PROXY and SURFCH4.

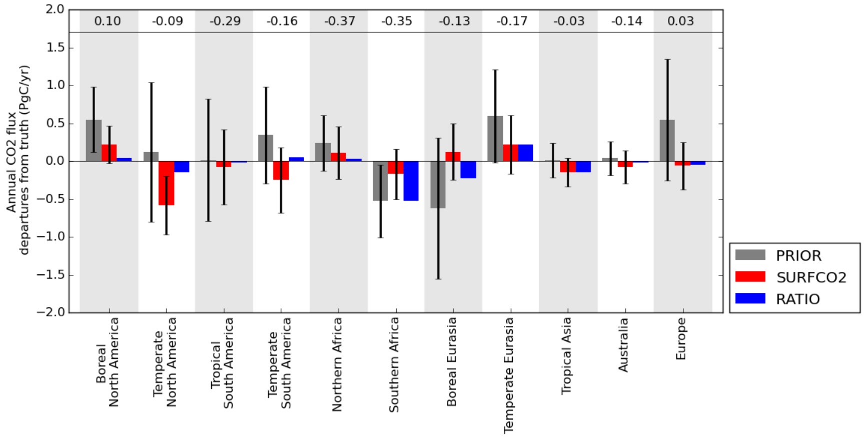

Figure 8. As Fig. 5 for the biosphere CO_2 fluxes in RATIO and SURFCO2 inversions.

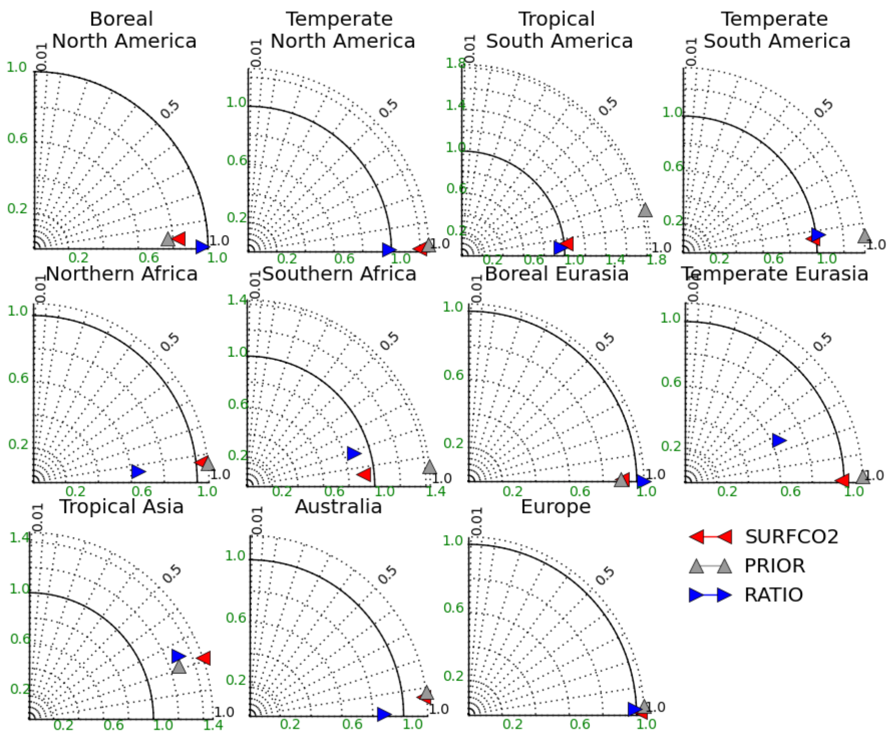

Figure 9. As Fig. 4 for the biosphere CO_2 fluxes in RATIO and SURFCO2 inversions.

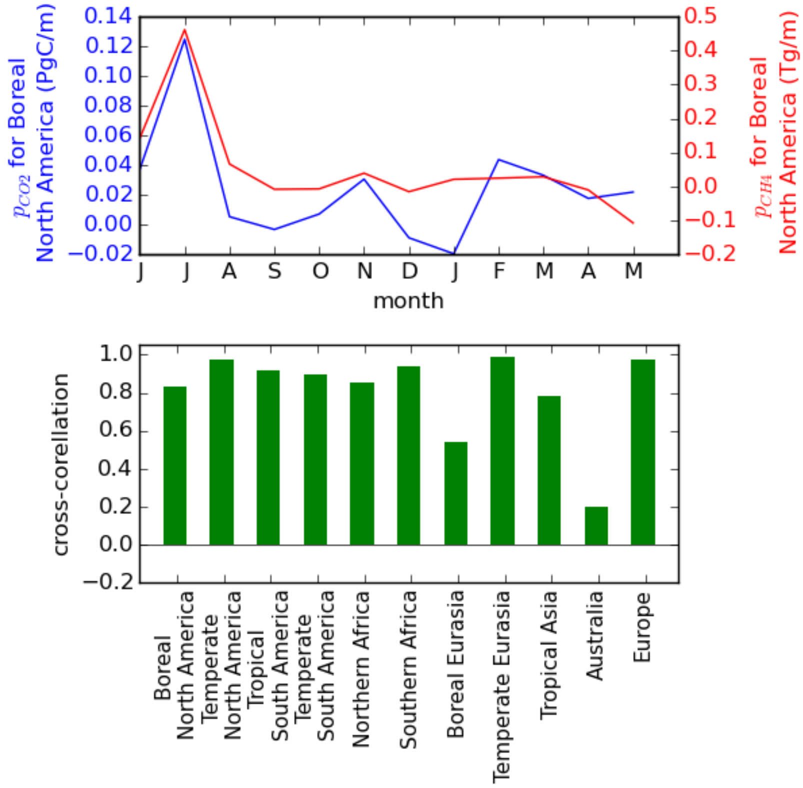

Figure 10. Top: $\boldsymbol{p}_{\mathrm{CH4}}$ and $\boldsymbol{p}_{\mathrm{CO2}}$ timeseries for Boreal North America. Bottom: cross-correlations between $\boldsymbol{p}_{\mathrm{CH4}}$ and $\boldsymbol{p}_{\mathrm{CO2}}$ for Transcom land regions (see Eq. 5).

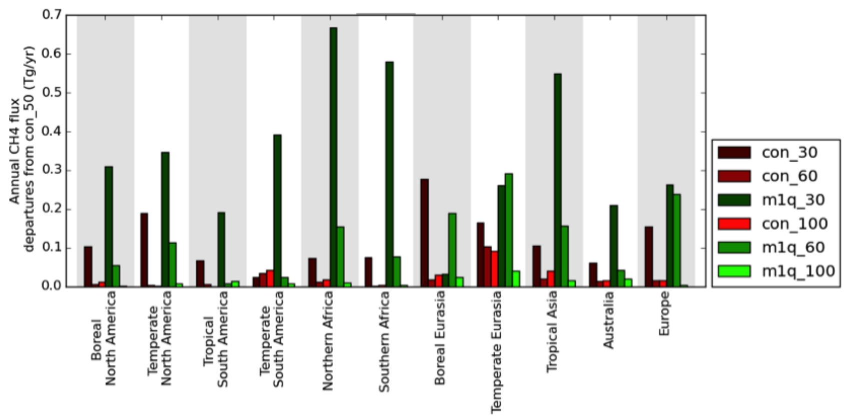

Figure 1.11. Absolute annual CH_4 flux departures of the inversion results from PROXY, which is run for 50 iterations using CONGRAD (see figure 7). The first part of label of each legend indicates the optimizer used for the inversion (m1q: M1QN3; con: CONGRAD), and the second part indicates number of iterations used.”